# InSb working standard radiometers

*G. P. Eppeldauer, A. L. Migdall and L. M. Hanssen*

**Abstract.** InSb radiometers have been developed and characterized for use as transfer standards at the National Institute of Standards and Technology (NIST). The InSb radiometers will hold a portion of the recently realized infrared spectral response scale of the NIST and will serve as working standards for the calibration of test detectors. These radiometers will measure radiant power or irradiance from 2 μm to 5.4 μm. They have a 17° field-of-view. The InSb detectors were selected for high shunt impedance to achieve high sensitivity. The transimpedance-gain, voltage-gain, and loop-gain of the current-to-voltage converters were optimized for optical radiation chopped at 40 Hz. At the peak response, the noise-equivalent-power is 0.6 pW in an electrical bandwidth of 0.3 Hz. The ratio of the dc ambient-background current to the ac noise-equivalent current is $10^7$. Spatial and angular responsivities, linearity, stability, and flashing were also characterized.

## 1. Introduction

The spectral-power response scale of the NIST from 2 μm to 20 μm [1, 2] has been realized on a cryogenic Si composite bolometer. The bolometer was calibrated against a primary-standard cryogenic radiometer at the NIST [3]. The infrared spectral response scale of the bolometer will be transferred to working-standard radiometers. The working standards, InSb and HgCdTe radiometers, will hold the infrared spectral response scale for everyday use. Test detectors will be calibrated against the working-standard radiometers. The design considerations and characterizations of the InSb working-standard radiometers are discussed here. The InSb radiometers are suitable to measure both radiant power and irradiance. They will be used either at the output of an infrared monochromator where the signal level is low [4], or to measure the irradiance from a monochromatic uniform source [5]. The design goals for these radiometers are high sensitivity (low noise) and wide dynamic-signal range, large detector area with a high-precision aperture at the front, uniform spatial response, cosine angular response, linearity, high photocurrent-to-voltage conversion accuracy at the signal chop frequency, and high stability.

## 2. Optical and mechanical design considerations

The radiometers were designed to minimize background signal, to include a high-precision aperture for irradiance measurements, and to maintain cosine-law response for use with incident beams away from normal incidence [5]. The liquid-nitrogen-cooled InSb photovoltaic detectors (4 mm diameter) were set 1 mm behind a 3.5 mm diameter aperture. The geometry of a long-snout InSb detector Dewar is shown in Figure 1. A second aperture situated about 50 mm from the high-precision aperture limits the field-of-view (FOV) to 17°, yielding an overall view angle of about 26°. A recess at the front of the FOV aperture-holder allows optional cold filters to be mounted. The high-precision aperture can be either underfilled or overfilled. These radiometers have been designed to measure either the $f/4$ output beam of a monochromator or the radiation from a laser-based, small-sphere source, underfilling the high-precision aperture for radiant-power-response calibrations and overfilling for irradiance measurements [5]. A baffle between the two apertures helps maintain cosine response by minimizing internal reflections. A 3° horizontally wedged window allows the detectors to be used for the measurement of either coherent or incoherent radiation. In a short-snout version, the separation between the apertures is only 7 mm, but external optics can be easily added to the Dewar.

## 3. Electronic design considerations

The detector preamplifier, which is integral with the detector Dewar, was designed for maximum sensitivity and current-to-voltage conversion accuracy at the chop frequency. The high shunt resistance, $R_s$, of the InSb detector reduces voltage gain, which minimizes amplification of input noise voltage (which is dominated by the $1/f$ noise of the operational amplifier [6]). Figure 2 shows the voltage gain, $G_V$, versus frequency [7].

G. P. Eppeldauer, A. L. Migdall and L. M. Hanssen: Optical Technology Division, National Institute of Standards and Technology, Gaithersburg, MD 20899, USA.

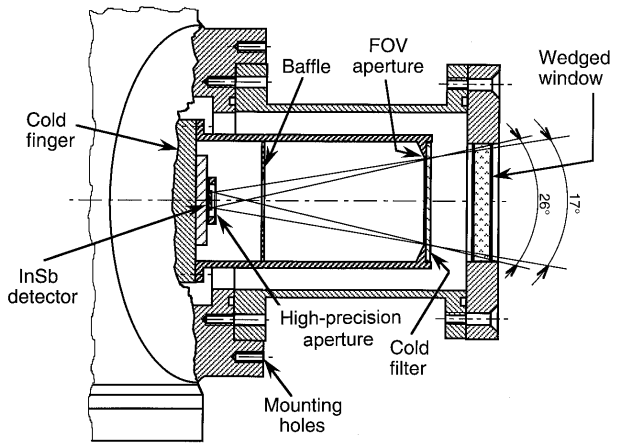


**Figure 1.** InSb Dewar mount with cold apertures and entrance window.

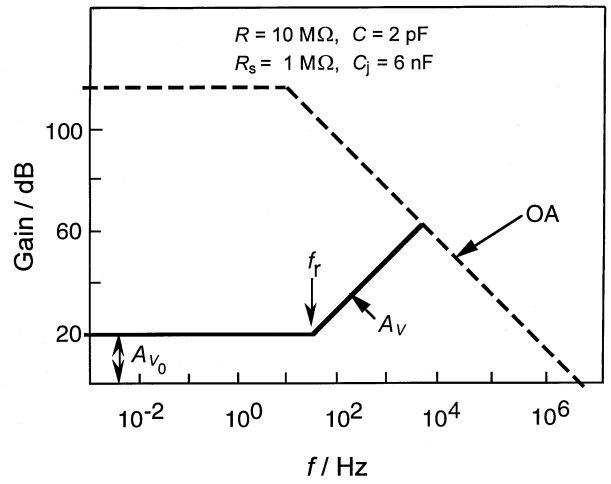


**Figure 2.** The voltage gain, $A_V$, of the InSb photodiode current-to-voltage converter is shown with the solid line. There is a noise-boosting effect from about 30 Hz to 8 kHz. The open-loop gain of the operational amplifier OA is shown with the dashed line.

An operational amplifier with low input-voltage noise and high dc-open-loop gain was selected for the photocurrent-to-voltage converter. The feedback resistor was limited to $R$ = 10 MΩ to avoid saturation by the dc radiation background. The time-constant determining the roll-on frequency $f_r$ is the product of two factors: the parallel resistance of $R$ and $R_s$ and the sum of $C$ and $C_j$ [8], the InSb junction capacitance. In our case, $f_r$ was dominated by the detector impedance ($R_s$ = 1 MΩ and $C_j$ = 6 nF). For $R$ = 10 MΩ, the low-frequency voltage gain, $A_{V_0} \approx 20$. The gain $A_V$ starts to increase at the chop frequency of approximately 40 Hz. At 4 kHz the noise voltage gain would be 100 times larger, assuming only stray capacitance (estimated to be $C$ = 2 pF).

Figure 3 shows the loop gain [9], $G_{loop}$, versus frequency with $R$ = 10 MΩ. The loop gain must be high at the chopping frequency to achieve accurate photocurrent-to-voltage conversion. The solid curve

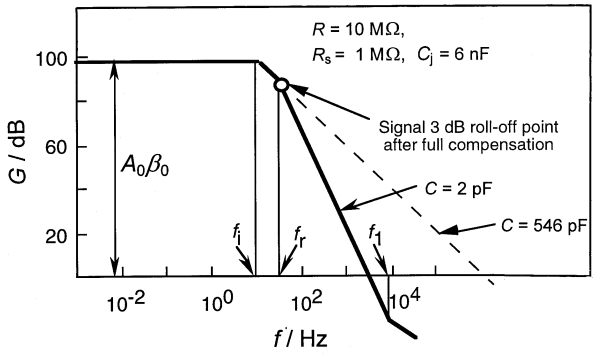


**Figure 3.** Loop gain, $G$, versus frequency. The solid curve is the uncompensated loop gain. The dashed curve shows the loop gain after full frequency compensation. The compensated 3 dB roll-off point of the signal response curve is shown with an open circle as it is matched to the dashed loop-gain curve. At low frequencies, $G = A_0\beta_0$, where $A_0$ is the dc open loop gain of the OA and $\beta_0$ is the dc feedback attenuation.

shows the uncompensated $C$ = 2 pF gain with a long – 40 dB/decade slope because $f_r$ and $f_i$ are close to each other and far from $f_1$. The frequency $f_i$ was determined from the dominant time-constant of the operational amplifier. In this figure, $f_r$ shows a roll-off as opposed to the roll-on of Figure 2. The frequency $f_1$ is determined by the time-constant ($RC$) of the feedback impedance. The loop gain reaches unity at about 3 kHz, which is lower than the 8 kHz signal 3 dB roll-off point calculated from the parallel $R$ = 10 MΩ and $C$ = 2 pF impedances [10]. In this case, the loop bandwidth is smaller than the signal bandwidth, which is a condition to be avoided. Also, two integrating time-constants that are close in frequency can cause gain peaking, yielding a sharp increase in amplitude at high frequencies and ringing.

An external 544 pF capacitor was connected in parallel to $R$ = 10 MΩ to achieve full frequency compensation. Tuning $f_1$ to $f_r$ cancels the roll-off at $f_r$ with the $f_1$ roll-on. The fully compensated ($f_r$ = $f_1$ = 30 Hz) loop-gain curve, indicated by the dashed line in Figure 3, also eliminates the noise-boosting effect shown in Figure 2 ($A_V = A_{V_0}$ for all loop frequencies). However, the original $f_1$ = 8 kHz 3 dB roll-off point decreased to 30 Hz. To operate on the plateau of the signal gain curve, the chop frequency must be a decade lower than the 3 dB point. A 3 Hz chopping frequency satisfies this requirement but because 3 Hz is much lower than the planned 40 Hz frequency, full compensation could not be made for the highest signal gains.

The chopping frequency can be increased if partial frequency compensations are performed for the high signal gains as shown in Figure 4. Increasing the 3 dB roll-off points to a minimum of 400 Hz allows a 40 Hz chopping frequency. For $R$ = 10 MΩ, the loop gain is still about 100 at the signal 3 dB roll-off point, yielding a 1% error in the current-to-voltage

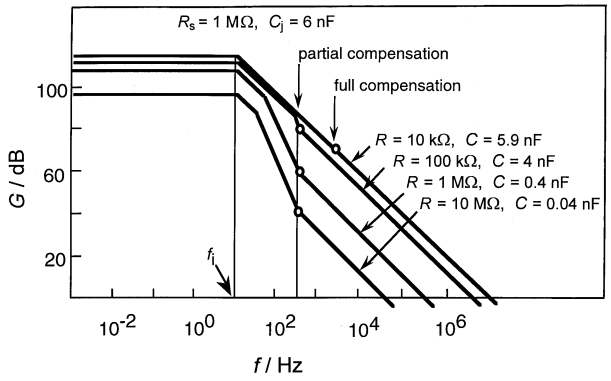


**Figure 4.** Partially and fully compensated loop-gain characteristics of the InSb photodiode current meter. The open circles show the 3 dB roll-off points of the photocurrent response functions matched to the loop-gain curves for each feedback resistor.

conversion. For the 1 MΩ and 100 kΩ feedback resistors, the loop gain increases further, resulting in higher signal-measurement accuracies. At $R$ = 10 kΩ, full compensation can be realized with the 3 dB point still above 400 Hz. The loop gain at this 3 dB point is about 4000. At 40 Hz, the loop gain equals or exceeds $3 \times 10^4$ for all $R$.

Figure 5 shows the voltage-gain curves for the partially and fully compensated signal-gain ranges. At 40 Hz, the noise-boosting effect is practically eliminated, even for the partially compensated signal-gain ranges.

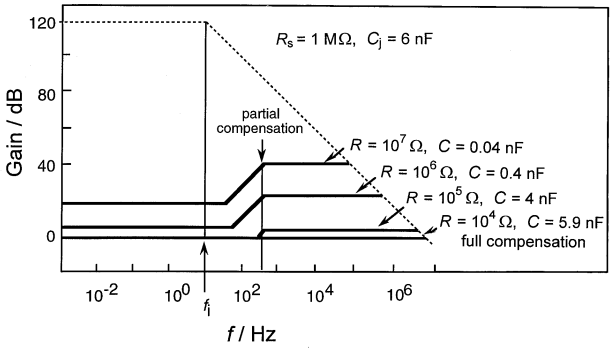


**Figure 5.** Voltage-gain curves (solid lines) for the partially and fully compensated signal gains of the InSb photocurrent meter. The signal chopping frequency is 40 Hz.

## 4. Radiometric characterizations

### *4.1 Responsivity versus time; flashing*

A 0.25 % response change was observed during the 15.5 h hold time of the Dewar (see Figure 6). This hold time depends on the Dewar vacuum level. Immediately after repumping, Dewar hold times in excess of 24 hours are possible. The 0.1 % instability in the second half of Figure 6 was measured after 18:00 h, when the environment of the setup was at its quietest. The radiation source was a quartz-halogen lamp, operated at half of its nominal 100 W operating power. The low temperature of the source and the 2 μm cut-on (order-sorting) filter were required to maintain the stability to within 0.1 % because radiation wavelengths shorter than about 2 μm produce response fluctuations due to trapped charges accumulating within the detector. These variations, seen as sudden jumps in the output level, are referred to as "flashing". Flashing can reach the level of a few percent if the visible/near-infrared radiation reaches the detector. Figure 7 shows the typical flashing seen when the tungsten-halogen lamp is used at its full 100 W power, providing more short-wave radiation. The radiation from the lamp passed through a monochromator set to 3.6 μm and a 2 μm cut-on filter. The $10^{-3}$ filter blocking was not enough to cut out the short-wave radiation from the detector, which had a dynamic range of nine decades. The fluctuations measured this way indicate the extreme sensitivity of flashing to

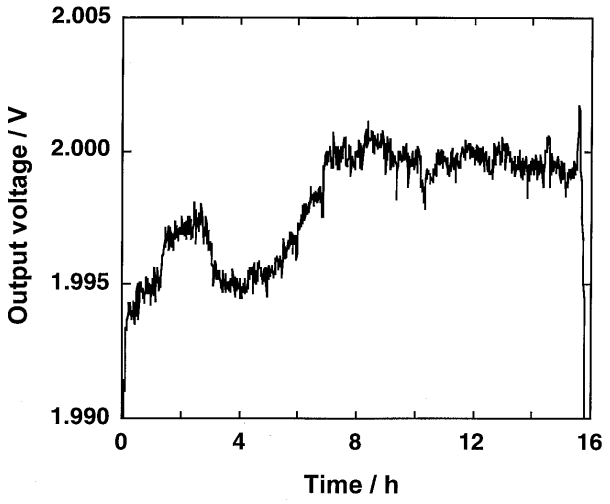


**Figure 6.** Test of InSb stability versus time at 3.8 μm.

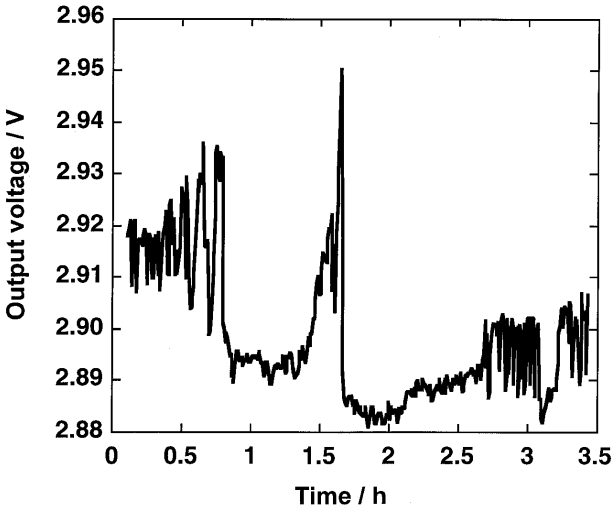


**Figure 7.** InSb flashing.

short-wave radiation. For accurate measurements, the flashing effect must be smaller than the expected uncertainties. This can be achieved by limiting the incident radiation below about 2 μm by employing cut-on filters and/or appropriate source-power distributions which have relatively low short-wavelength output. Flashing may also be reduced by better detector design, such as by applying an integrated aperture on the InSb chip outside the photosensitive area [11]. The InSb detector output should be monitored for a period of about 1 h to verify that flashing effects are below the desired level.

### *4.2 Responsivity versus frequency*

The normalized, measured, frequency-dependent signal responsivities of the InSb radiometers at gains of $10^4$, $10^5$, and $10^6$ V/A are shown in Figure 8. The results are in good agreement with the design values shown in Figure 4. The 3 dB point could not be measured at gain $10^7$ V/A because no cold filter was installed in front of the detector. The detector measured the background radiation with its full broadband responsivity, resulting in a too-large dc background current for this signal-gain range.

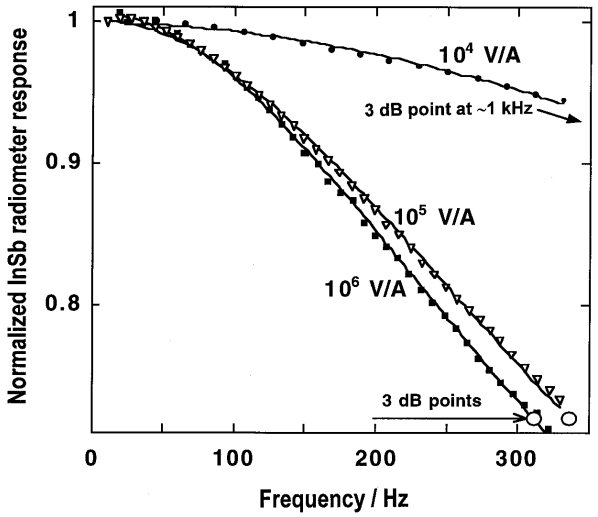


**Figure 8.** InSb radiometer response versus frequency, normalized to unity at dc, for three different gain settings. One-time-constant response curves are fitted (solid lines) to the measured data points.

### *4.3 Responsivity nonlinearity*

The nonlinearity of the InSb radiometer was tested by comparison with a calibrated transfer-standard Ge detector over a range of input power levels. The measurements were made using a chopped diode-laser beam at 1.3 μm where the two detectors overlap spectrally. Neutral-density filters inserted into the beam were used to vary the radiant power level. The two detectors were substituted for each other.

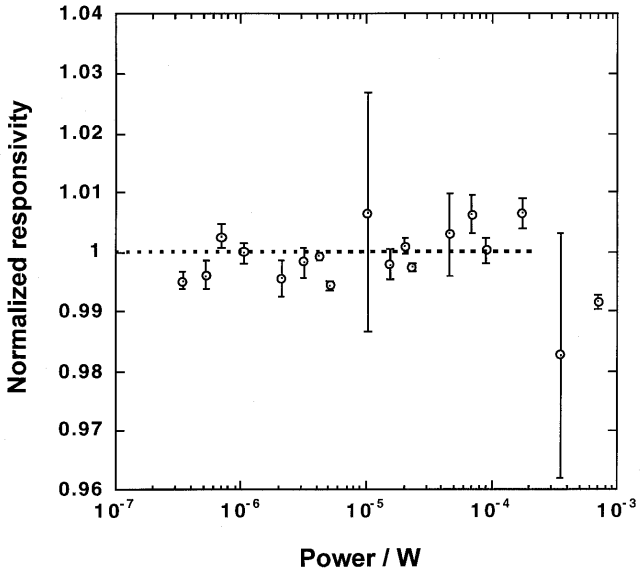


**Figure 9.** Ratios of InSb to Ge response (for identical radiant-power inputs) divided by a constant to yield a mean value near unity (see text).

Figure 9 shows the InSb to Ge response ratios measured versus radiant power (the ratios have been normalized by the average value over the range $2 \times 10^{-7}$ W to $2 \times 10^{-4}$ W). The uncertainty bars in the figure represent only the standard deviation of repeated measurements. If we exclude the two points in Figure 9 which show very large relative standard deviations owing to flashing (Section 4.1), the estimated overall relative standard uncertainty for the entire measurement range is 1%. This includes major contributions from flashing, the lock-in-amplifier gain calibration, and the current-to-voltage amplifier calibration. The InSb detector is linear up to about 0.1 mW with evidence of about 1% nonlinearity at 0.75 mW.

### *4.4 Dynamic range*

The noise component from the input-voltage noise density of the operational amplifier was calculated at 43 Hz. At $R$ = 1 MΩ, where the voltage gain was small ($A_V$ = 2 as shown in Figure 5), the equivalent photocurrent noise was 0.06 pA/Hz$^{-1/2}$. The equivalent photocurrent of the Johnson noise was 0.1 pA/Hz$^{-1/2}$. The $1/f$ noise component was calculated from the amplifier catalogue for the 0.1 Hz to 10 Hz bandwidth. The equivalent effective photocurrent of this noise is about 0.6 pA/Hz$^{-1/2}$. At 43 Hz the $1/f$ noise is significantly lower.

The RMS total noise current was measured with an electrical bandwidth of 0.3 Hz at 43 Hz, at different wavelength settings of a monochromator. The total noise scale (left $y$-axis of Figure 10) indicates low background signal at 2 μm, and a large $1/f$ noise component. No heated IR source was used in this measurement. The background radiation was chopped

at 43 Hz, producing the detector ac mean current (right $y$-axis of Figure 10). The total current noise increased by more than a factor of two as the monochromator was tuned from 2 μm to 5 μm. The steep slope of the solid curve shows the background noise component increasing with wavelength. The total noise current was about 30 times smaller than the mean ac background-produced detector current at 5 μm. The dominant component of the total noise current in the long-wavelength range is the shot noise of the dc ambient background current. In an independent test, a 13.4 μA dc background current was measured without any spectral selection of the input radiation. The current noise, calculated from this dc background current, was 1.13 pA, just slightly lower than the total noise current observed at the longest wavelength measured. The total noise current of the detector determines the limiting noise-equivalent power (NEP) of the InSb radiometer. The measured NEP at the peak response (2 A/W) was 0.6 pW (RMS) in an electrical bandwidth of 0.3 Hz. The ratio of the dc ambient background current to the RMS total noise current was about $10^7$.

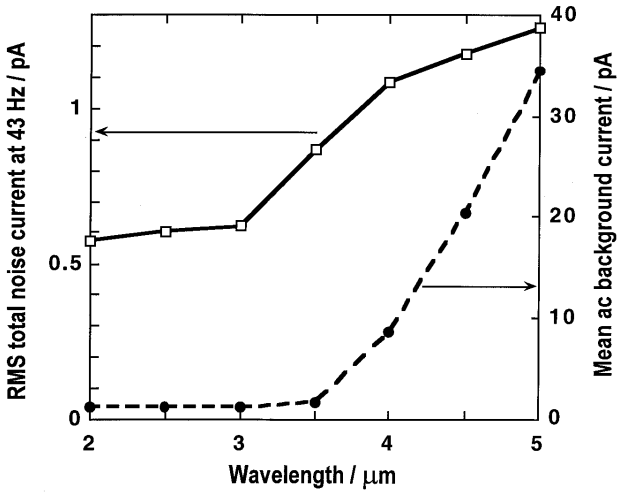


**Figure 10.** Total noise and ac background current versus monochromator wavelength.

The maximum detector current can be measured at a gain of $10^4$ V/A. A 1 mA maximum current on the 10 V full-scale output corresponds to a maximum measurable radiant power of 0.5 mW at the InSb peak responsivity, and thus the dynamic range of the InSb radiometer is nine decades.

### *4.5 Spatial/angular responsivity*

Spatial-response variations were measured along the horizontal and vertical diameters of the InSb detectors. Figure 11 shows a variation of less than 2% in the horizontal scan within the 3.5 mm diameter of the high-precision aperture. The angular response was tested by rotating the detector around its vertical axis. The axis of rotation was close to the centre of the high-precision

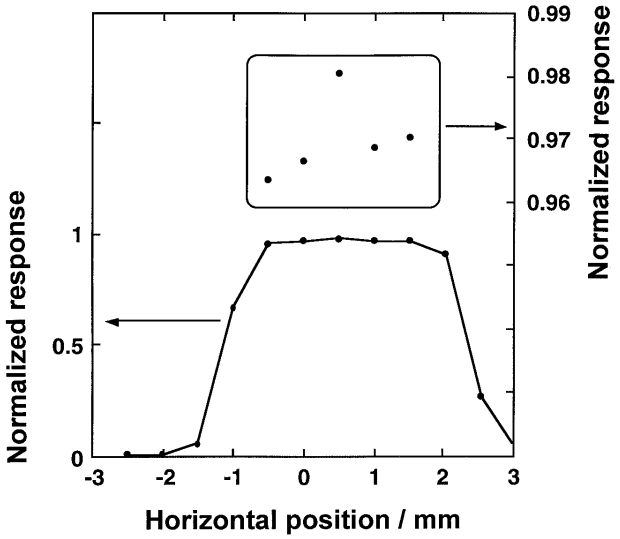


**Figure 11.** InSb radiometer: variation in horizontal spatial response. The inset shows the data on the expanded scale marked on the right.

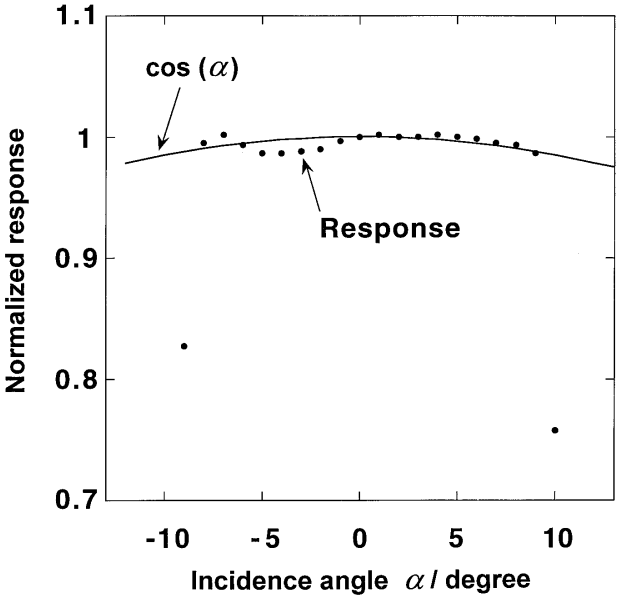


**Figure 12.** InSb radiometer: variation in angular response.

aperture. The measurement results shown in Figure 12 were obtained using a point source 1.2 m from the detector. The measured field-of-view is 17°. The maximum deviation of the measured angular response from a cosine law is ± 1%. There was no baffle installed in the FOV-limiting tube during this measurement. The slight measured deviation may indicate a need for a baffle in the input beam, as shown in Figure 1.

## 5. Conclusion

Standard-quality InSb radiometers have been developed as working standards to hold the spectral response scale of the NIST between 2 μm and 5.4 μm. The

radiometers can measure radiant power or irradiance in a signal range of nine decades. The NEP is approximately 1 pW/Hz$^{1/2}$. Signal (photocurrent)-gain, voltage-gain, and loop-gain were optimized for operation at approximately 40 Hz. The area of the high-precision aperture is 0.1 cm$^2$, with an FOV of 17°. The spatial-response non-uniformity and the deviation of the angular response from a cosine function are about 1%. The response non-linearity at the high-signal end (about 0.7 mW) is about 1%. The 8 h stability of the radiometers is about 0.1%.

## References


1. Eppeldauer G., Migdall A. L., Gentile T. R., Cromer C. L., Absolute response calibration of a transfer standard cryogenic bolometer, In *Photodetectors and Power Meters II* (Edited by K. Muray and K. J. Kaufmann), *Proc. SPIE*, 1995, **2550**, 36-46.
2. Migdall A., Eppeldauer G., Realization of an infrared spectral radiant power response scale on a cryogenic bolometer, *Metrologia*, 1998, **35**, 307-315.
3. Gentile T. R., Houston J. M., Hardis J. E., Cromer C. L., Parr A. C., National Institute of Standards and Technology high accuracy cryogenic radiometer, *Appl. Opt.*, 1996, **35**, 1056-1068.
4. Migdall A., Eppeldauer G., Cromer C., IR detector spectral responsivity calibration facility at NIST, In *Cryogenic Optical Systems and Instruments VI* (Edited by J. B. Heaney and L. G. Burriesci), *Proc. SPIE*, 1994, **2227**, 46-53.
5. Eppeldauer G., Near Infrared Radiometer Standards, In *Optical Radiation Measurements III* (Edited by J. M. Palmer), *Proc. SPIE*, 1996, **2815**, 42-54.
6. Eppeldauer G., Hardis J., Fourteen-decade Photocurrent Measurements with Large-area Silicon Photodiodes at Room Temperature, *Appl. Opt.*, 1991, **30**, 3091-3099.
7. Eppeldauer G., Electronic Characteristics of Ge and InGaAs Radiometers, In *Infrared Technology and Applications XXIII, Proc. SPIE*, 1997, **3061**, 833-838.
8. *Product Data Book of Burr-Brown*, Tucson, Arizona, Burr-Brown Corporation, 1984, 1-38.
9. Horowitz P., Hill W., *The Art of Electronics*, Cambridge, Cambridge University Press, 1987, 127-128.
10. Rieke G. H., *Detection of Light: from the Ultraviolet to the Submillimeter*, Cambridge, Cambridge University Press, 1994, 143 p.
11. EG&G Judson Company, personal communication, 1997.